

ARTICLE

Open Access

Formation and fluorescent mechanism of red emissive carbon dots from *o*-phenylenediamine and catechol system

Pengfei Li¹, Shanshan Xue¹, Lu Sun¹, Xupeng Zong¹, Li An¹, Dan Qu¹, Xiayan Wang¹ and Zaicheng Sun¹✉

Abstract

Carbon dots (CDs) as the advancing fluorescent carbon nanomaterial have superior potential and prospective. However, the ambiguous photoluminescence (PL) mechanism and intricate structure-function relationship become the greatest hindrances in the development and applications of CDs. Herein, red emissive CDs were synthesized in high yield from *o*-phenylenediamine (oPD) and catechol (CAT). The PL mechanism of the CDs is considered as the molecular state fluorophores because 5,14-dihydroquinoxalino[2,3-*b*] phenazine (DHQP) is separated and exhibits the same PL properties and behavior as the CDs. These include the peak position and shape of the PL emission and PL excitation and the emission dependence on pH and solvent polarity. Both of them display close PL lifetime decays. Based on these, we deduce that DHQP is the fluorophore of the red emissive CDs and the PL mechanism of CDs is similar to DHQP. During the PL emission of CDs, the electron of the molecule state can transfer to CDs. The formation process of DHQP is further confirmed by the reaction intermediates (phthalazine, dimers) and oPD. These findings provide insights into the PL mechanism of this type of CDs and may guide the further development of tunable CDs for tailored properties.

Introduction

Carbon dots (CDs) as a new class of fluorescent carbon nanomaterial has attracted much more attention progress due to their low cost, high stability, low toxicity, high biocompatibility, easy surface modification, and tunable fluorescent properties since it was discovered in 2004^{1–3}. Those unique properties enable it to have fantastic application potential in bioimaging, biological probe, biomedicine, catalysis, light-emitting diodes (LEDs), and so on^{4–12}. Knowledge of their PL mechanisms is of significance in guiding the synthesis and promoting applications of CDs with tunable PL emissions. However, the intrinsic PL emission mechanism remains unclear, and a unified mechanism has not been achieved because of differences in particle structures. Thus, the revealing of

CDs structure and PL mechanism is very significant in promoting its development and applications. Currently, the most acceptable PL mechanism can be described into three categories: surface state, carbon core state, and molecular state². The carbon core state refers to the π - π^* electron transitions of the conjugated sp^2 domains^{4,13,14}. The size of the isolated sp^2 subdomain determines the emission of CDs¹⁵. The characteristics of the surface state are that the surface functional groups connecting with the carbon backbone control the electron structures and energy level by hybridization. The luminescence can be adjusted by altering types and contents of surface functional groups^{16,17} or the heteroatoms doping^{18,19}. The molecule state refers to the molecular fluorophores or their aggregate which is connected with CDs dominated by the fluorescence, and it generally endows CDs with a strong PL and a high PLQY^{20,21}. The CDs from citric acid (CA) are well investigated and analyzed, ICPA (imidazo[1,2-*a*]pyridine-7-carboxylic acid) was considered as

Correspondence: Zaicheng Sun (sunzc@bjut.edu.cn)

¹Center of Excellence for Environmental Safety and Biological Effects, Beijing Key Laboratory for Green Catalysis and Separation, Department of Chemistry, Beijing University of Technology, 100124 Beijing, China

© The Author(s) 2022



Open Access This article is licensed under a Creative Commons Attribution 4.0 International License, which permits use, sharing, adaptation, distribution and reproduction in any medium or format, as long as you give appropriate credit to the original author(s) and the source, provide a link to the Creative Commons license, and indicate if changes were made. The images or other third party material in this article are included in the article's Creative Commons license, unless indicated otherwise in a credit line to the material. If material is not included in the article's Creative Commons license and your intended use is not permitted by statutory regulation or exceeds the permitted use, you will need to obtain permission directly from the copyright holder. To view a copy of this license, visit <http://creativecommons.org/licenses/by/4.0/>.

a fluorescent molecule crosslinked with the CDs core, that is the strong blue PL center of the CDs from CA and ethylenediamine^{20,22}. In general, different CDs synthesized by different routes possess structural features, they demonstrate different PL properties and mechanisms. However, the CDs obtained from aromatic molecules are rarely investigated.

Red emissive CDs not only can penetrate tissue deeply to avoid auto-fluorescence of organisms^{5,23}, but also is a significant component of the white light-emitting diodes (WLEDs)²⁴, it has been recognized as a key requirement to promote the practical applications of CDs in most fields²⁵. Small aromatic molecules, as the common precursors, can generate large sp^2 domains with a narrow energy gap, which is beneficial to tuning the emission and excitation toward long wavelength²⁶. However, the PL mechanism of red emissive CDs prepared by aromatic molecules has always been controversial. Lin and coworkers through the solvothermal method synthesized red, green, and blue luminescence CDs with *p*-phenylenediamine (pPD), *o*-phenylenediamine (oPD), and *m*-phenylenediamine (mPD) as precursors, respectively. Simultaneously, the red emission for the CDs is attributed to the bigger particle size and more nitrogen content²⁷. Xiong group used oPD as a precursor to prepare full-color emissive CDs by solvent-free approach, with the increased conclusion that the size of sp^2 -conjugated domains and the content of graphitic nitrogen contribute to red emission of CDs²⁸. Zhong and coworkers supposed that newly emerged 2,3-diaminophenazine (DAPN) fluorophore interaction with carbon structure and its protonation directly determine the molecular state fluorescence of CDs²⁹. Neeraj Soni et al. obtained red, green, and blue emissive components isolated and purified from CDs solution by column chromatographic. The red PL is attributed to a molecular fluorophore, quinoxalino[2,3-*b*]phenazine-2,3-diamine (QXPDA), the QXPDA attached to the surface of core carbon, and aggregated together, which led to green and blue emission³⁰. Overall, the red PL emission mechanism, which keeps mystery, strongly depends on the chemical structure of fluorophores. The defined chemical structure will promote the understanding of the PL of CDs.

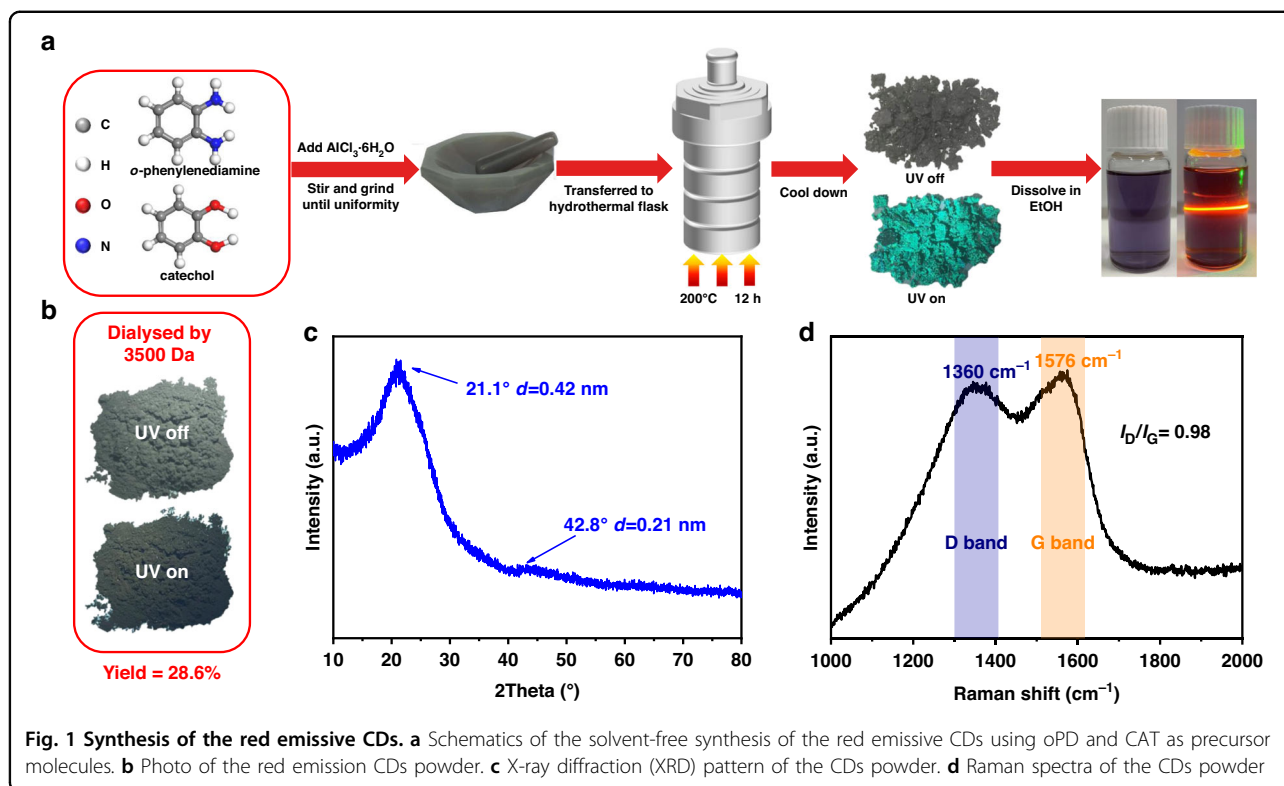
Herein, we synthesized red emissive CDs with high yield from oPD and catechol (CAT) catalyzed by aluminum chloride hexahydrates ($AlCl_3 \cdot 6H_2O$) through the solvent-free method. To reveal the PL mechanism of red emissive CDs, the reaction intermediates are investigated by high-performance liquid chromatography-mass spectroscopy (HPLC-MS), proton nuclear magnetic resonance (1H NMR), and PL spectroscopies. It discloses that molecular organic species of 5,14-dihydroquinoxalino[2,3-*b*]phenazine (DHQP) is an important intermediate, which exhibits similar PL properties as CDs.

That implies that DHQP is the fluorophore of red emissive CDs, the PL mechanism was proposed to follow the molecular state PL. Furthermore, the forming process of DHQP is proposed. The oPD and CAT form phthalazine and 2,3-diaminophenazine (2,3-DAPN) by dehydrated reaction, and then 2,3-DAPN and phenazine reaction with oPD to produce fluorescent molecule (DHQP). With prolonging the reaction time, graphitic CDs fragments gradually form by carbonizing these conjugated molecules, DHQP unit is remained during the carbonization, either incorporated into the carbon framework or linked to the surface of CDs. The remained DHQP unit on the carbon core, as the molecular fluorophore, emits a similar red light to the DHQP molecule. However, CDs exhibit higher solubility and photo and thermal stability than DHQP. In the fluorescence mechanism of CDs, the excited electron of DHQP can transfer to the CDs' energy level, leading to the maximum excitation wavelength of CDs redshift to 540 nm. This discovery of the PL mechanism has specific directive significance for the synthesis and applications of CDs.

Results

Characterization of red emission CDs

In this work, red emissive CDs were synthesized from oPD and CAT as the precursors catalyzed by $AlCl_3$ by the solvent-free method. As shown in Fig. 1a, the as-prepared product shows intense cyan solid-state fluorescence under ultraviolet light. However, the X-ray diffraction (XRD) pattern exhibits multiple sharp peaks (Fig. S1a), which indicates the as-prepared product contains a lot of crystalline species. The PL spectra exhibit two strong emissions at 600 nm and 650 nm under the excitation at 520 nm (Fig. S1b, c). To remove impurities, the as-prepared product was dissolved in ethanol for dialysis purification with 3500 Da molecular weight cut-off in DI water till no fluorescence was detected in dialysate. A gray powder can be obtained and lost its cyan solid-state fluorescence (Fig. 1b) after dialysis. The yield of CDs prepared by this method can reach 28.6%, which is much higher than that of the traditional hydrothermal or solvothermal methods. The XRD pattern (Fig. 1c) depicts two peaks at 21.1° and 42.8° , which correspond to (002) and (100) of graphitic structure. The peak at 21° corresponds to d spacing of 0.42 nm, which is larger than the normal d spacing of 0.35 nm of the graphitic (002) crystal plane. This implies that the functional groups may exist on the layer surface or edge. Figure 1d shows the typical Raman spectra of the CDs, which exhibit two peaks at 1360 cm^{-1} and 1576 cm^{-1} that contributed from the disordered (D band) and graphite (G band) of carbon materials. The ratio of the I_D/I_G is 0.98 indicating the CDs possess a degree of graphitization³¹.

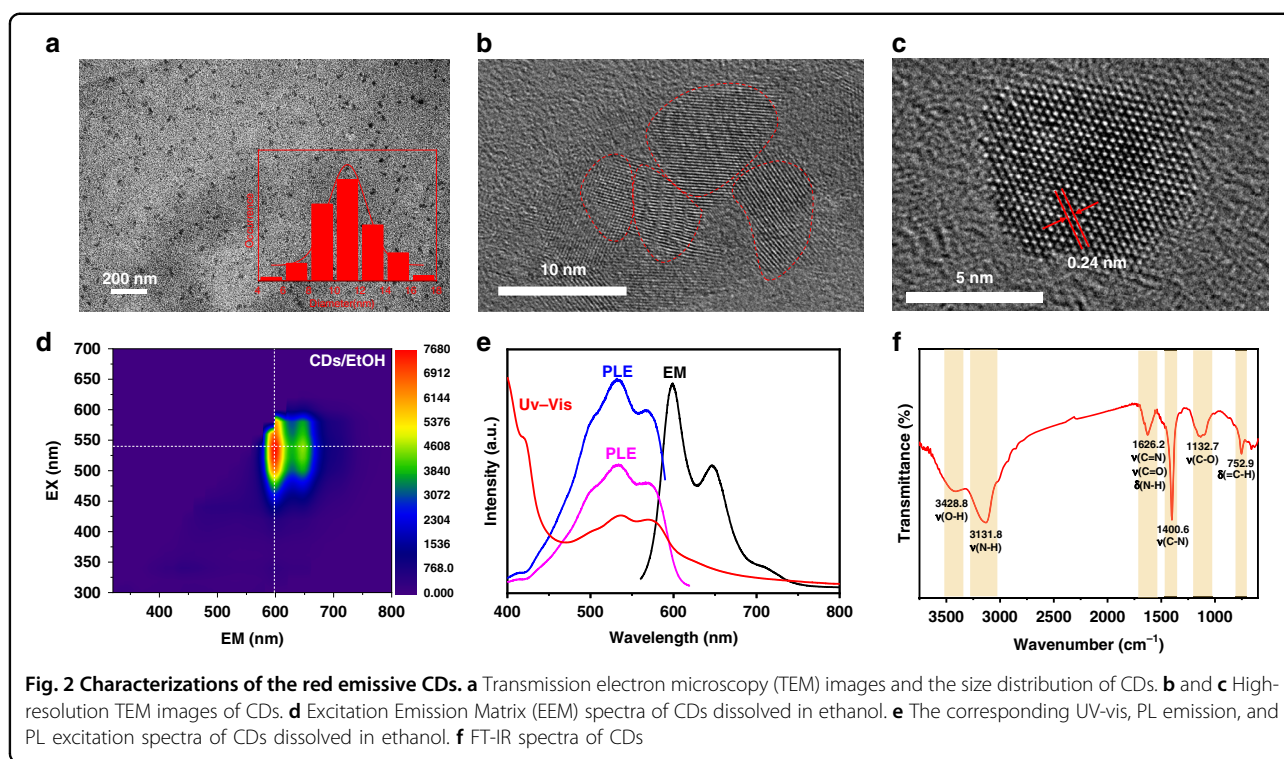


Transmission electron microscopy (TEM) images (Fig. 2a–c) disclose that obtained CDs are uniform and have a particle size of 10.8 ± 2.3 nm. The high-resolution (HR) TEM images of the CDs disclose the lattice fringe distance was 0.24 nm which is attributed to the d spacing of the graphene (100). Figure 2b shows the CDs tend to form an aggregation in the solid state. Figure 2d depicts the excitation-emission matrix (EEM) spectra of CDs in ethanol, which mainly exhibit a 600 nm and 650 nm PL emission center. UV-vis, PL emission and PL excitation (PLE) spectra (Fig. 2e) indicate the emissions at 600 nm and 650 nm originate from the transition of absorption bands at 500, 530, and 570 nm. The absolute photoluminescence quantum yield (QY) is 2.65%. Fourier transform infrared (FTIR) spectra of CDs (Fig. 2e) presents the peaks at 3329, 3132, 1626, 1401, and 1133 cm^{-1} are attributed to the stretching vibrations of O-H, N-H, C = N (or C = O), C-N, and C-O, besides, the peak at 753 cm^{-1} can be assigned to the bending vibration of C-H of the benzene ring. In Fig. S2, the X-ray photoelectron spectroscopy (XPS) analyzed the chemical composition of the CDs. Full-scan XPS spectra (Fig. S2a) reveal the consistency of carbon (C), nitrogen (N), and oxygen (O) elements with an atomic fraction of 85.29%, 9.77%, and 4.84%, respectively. High-resolution XPS spectra of C1s, N1s, and O1s are shown in Fig. S2b, c, d, respectively. The C1s XPS spectra can be deconvoluted into four components: C = C/C-C (284.8 eV),

C-N (285.8 eV), C = N (287.2 eV), and C = O (298.0 eV). The N1s XPS spectra can be converted into three types of nitrogen: pyridinic N (C-N = C, 399.1 eV), pyrrolic N (C-NH-C or N-(C)₃, 400.6 eV), and amine N (N-H, 402.0 eV). Only C = O (532.2 eV) can be observed in O1s XPS spectra^{28,29}. These results reveal that dehydration and deamination happen in the formation process of CDs.

Origin of red emission

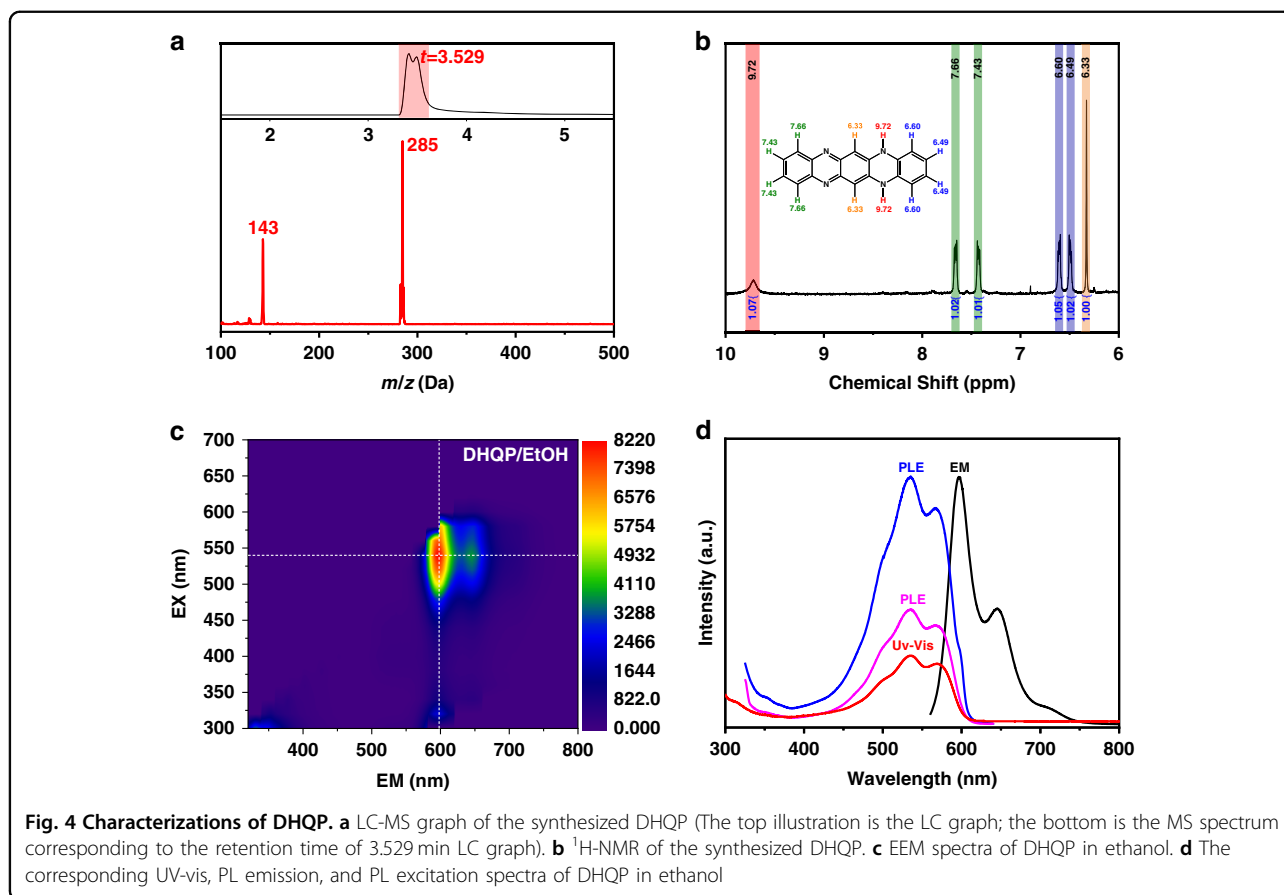
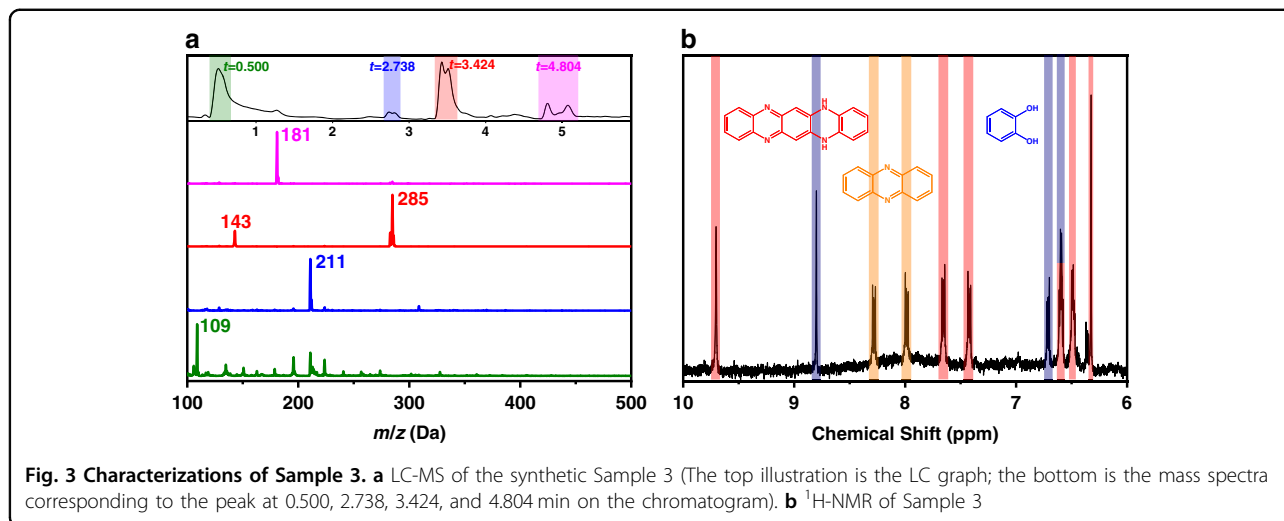
Although no solvent was added, the reaction between oPD and CAT happens in homogenous liquid due to the melting points of both oPD and CAT being $\sim 103^\circ\text{C}$. To our surprise, when oPD and CAT ethanol solution are mixed at room temperature by the molar ratio of 1:1, the mixed solution gradually turned from colorless to reddish and exhibited red emission with excitation by 532 nm laser (Fig. S3a). EEM spectra, PL emission, and PL excitation spectra show that the emission peaks of the mixed solution are 600 nm and 650 nm, which are very close to the CDs' emission. Similar optical properties guide us to consider a red emissive molecule formed in the solution, which is the fluorophores of red emissive CDs (Fig. S3d). Consequently, the PL mechanism of this type of CDs should belong to molecule state fluorescent. However, a trace amount of product results in it being hard to determine the molecular structure of the formed molecule.



To investigate the chemical structure of the fluorescent, the oPD and CAT mixture was heated to different temperatures without $\text{AlCl}_3 \cdot 6\text{H}_2\text{O}$ for 6 h to slow down the reaction. The intermediates were investigated by high-performance liquid chromatography-mass spectrometry (HPLC-MS) and Proton Nuclear Magnetic Resonance ($^1\text{H-NMR}$). Figure S4a shows the HPLC-MS of the product synthesized at 100°C for 6 h without any further purification (Sample 1). In this mild reaction condition, melt oPD and CAT react to each other. The HPLC graph depicts a strong peak at 0.552 min and two weak peaks at 2.739 min and 3.439 min. The corresponding MS spectra exhibit the peaks of m/z at 109, 211, and 285 for the fraction at the retention time of 0.552, 2.739, and 3.439 min, respectively. The estimated molecules are unreacted oPD/CAT, 2,3-DAPN, and DHQP, respectively. $^1\text{H NMR}$ spectrum of the product (Fig. S4d) displays 4 equal intensity chemical shifts at 6.37, 6.49, 6.60, and 6.72 ppm, and one peak at 8.83 ppm and one at 4.39 ppm. The integration area ratio of these peaks is 1:1:1:1:2. The chemical shifts and integration of these peaks completely match the $^1\text{H NMR}$ peaks of oPD and CAT. Consequently, these peaks are assigned to the H on the unreacted oPD and CAT. Compare to the CAT, the peak at 8.83 ppm ($-\text{OH}$) has changed its shape from the sharp one to a wide weak peak implying that the proton turns more active³². Although 2,3-DAPN and DHQP were detected by HPLC-MS, it is hard to be detected by $^1\text{H NMR}$ due to the amount of these being low.

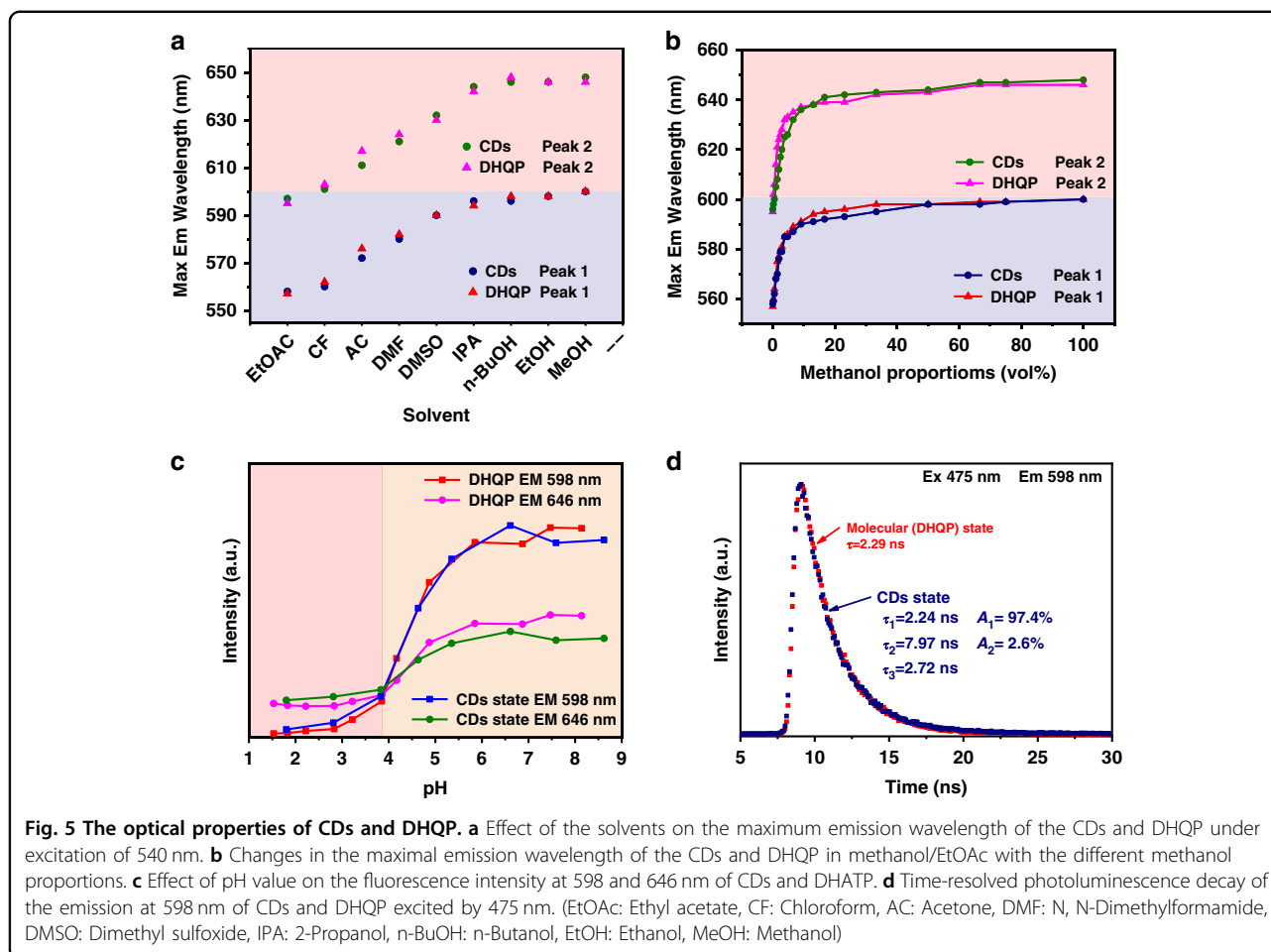
Figure S4b presents the HPLC graph and the corresponding MS spectra of different fractions for Sample 2 prepared at 200°C for 12 h. The relative intensity of peaks at both 2.739 min and 3.439 min increases in HPLC spectra (Fig. S4b). In addition, two new peaks appear at the retention time of 4.804 and 5.063 min, the corresponding MS spectra display the m/z of 181. That retention time and MS peak are the same as those of pure phthalazine (Fig. S4c). $^1\text{H NMR}$ spectrum of phthalazine (Fig. S4d) exhibited two peaks at $\delta = 7.99$ ppm (dd, $J_1 = 6.8$, $J_2 = 3.4$ Hz, 4H) and 8.28 ppm (dd, $J_1 = 6.7$, $J_2 = 3.4$ Hz, 4H). The same peaks are observed in the green trace (Fig. S4d) implying that phthalazine and reactants are the main product. The other two fractions in HPLC-MS do not detect in the $^1\text{H NMR}$ spectra of the as-prepared sample. The as-prepared product needs to be further purified to obtain Sample 3.

After purification, the HPLC-MS and $^1\text{H NMR}$ spectra are shown in Fig. 3. The fraction at $t = 3.424$ min significantly increase (Fig. 3a) and the fraction at $t = 4.804$ min decreased due to the impurities being removed. In the corresponding mass spectrometry, The peak at m/z of 285 is attributed to the DHQP $[\text{M} + \text{H}]^+$. A peak of m/z at 143 emerged, it could correspond to the DHQP molecule carrying 2 charges $([\text{M} + 2\text{H}]^{2+})$. The $^1\text{H NMR}$ spectrum of Sample 3 is presented in Fig. 3b. To determine the attribution of these chemical shifts, DHQP was synthesized with oPD and 2,3-DAPN as a precursor (the detailed synthetic method is given in the ESI). HPLC-



MS and $^1\text{H-NMR}$ were carried out to identify the structure of the synthetic product. The chromatogram spectrum (Fig. 4a) presents a strong signal at 3.529 min, and the corresponding MS spectra emerge two peaks at 285, and 143 Da, which all are characteristic MS peaks of DHQP. The $^1\text{H NMR}$ spectrum (Fig. 4b) presents the following peaks: 6.32 (s, 2H), 6.49 (dd, $J_1 = 5.7$,

$J_2 = 3.4$ Hz, 2H), 6.60 (dd, $J_1 = 7.3$, $J_2 = 3.7$ Hz, 2H), 7.42 (dd, $J_1 = 6.5$, $J_2 = 3.5$ Hz, 2H), 7.66 (dd, $J_1 = 6.5$, $J_2 = 3.5$ Hz, 2H), and 9.71 (s, 2H). Compared to $^1\text{H-NMR}$ spectra of pure DHQP (Fig. 4b), the peaks at 6.32 ppm, 6.45–6.52 ppm, 6.55–6.63 ppm, 7.42 ppm, 7.66 ppm, and 9.70 ppm are contributed to the DHQP in reaction intermediates (Fig. 3b). The chemical shifts at 7.99 ppm



and 8.28 ppm are assigned to the phthalazine as well. The peaks at 8.80 ppm and 6.71 ppm are assigned to the H on the -OH and benzene of CAT, the other chemical shift of CAT is at 6.60 ppm, which is coincident with the characteristic chemical peak of DHQP. Based on the above results, the fluorophores of CDs might be the above intermediate molecules such as phenazine, 2,3-DAPN, or DHQP.

To confirm the fluorophores of the CDs, we measured the optical properties of commercial phenazine and 2,3-DAPN (Fig. S5). Phenazine displays a very weak PL emission. The quantum yields are as low as 0.27% in ethanol. The maximum emission of 2,3-DAPN is at 534 nm with an excitation of 420 nm. The PL QY of 2,3-DAPN in ethanol was measured to be 7.05%. These indicate phenazine and 2,3-DAPN are not fluorophores of the CDs. To determine whether or not DHQP is the fluorophore of CDs, The EEM of DHQP is presented in Fig. 4c, which clearly shows two emission centers at 600 nm and 650 nm, which are the same as those of CDs. But the PL QY is about 26.50%, much higher than CDs. UV-vis, PL, and PLE spectra of DHQP are displayed in

Fig. 4d, which exhibits two PL emission peaks at 600 and 650 nm, which originate from the transition of absorbance bands at 500, 530, and 570 nm. The PL spectra of DHQP exhibit high similarity to the PL spectra of CDs. We infer that DHQP is the fluorophore of this type of CDs.

To verify the fluorophore of the CDs is DHQP, we comparative investigate the effect of solvents, pH, and time-resolved PL on the optical properties of CDs and DHQP. Figure S6a, b depict the PL spectra of DHQP and CDs in the common solvent including ethyl acetate (EtOAc), chloroform (CF), acetone (ACE), N, N -dimethylformamide (DMF), dimethyl sulfoxide (DMSO), isopropanol (IPA), n-butyl alcohol (BuOH), ethanol (EtOH), methanol (MeOH). Both CDs and DHQP show a similar shift of two emission peaks (Fig. S5a, b). Figure 5a presents the changing trend of maximal emission with solvent polarity. With decreasing the polarity of the solvent, the maximum emission blue-shift from 600 nm for MeOH with a relative polarity of 0.762 to 558 nm for EtOAc with a relative polarity of 0.228. More important is both CDs and DHQP keep the same pace with changing the relative polarity of the solvent. The phenomenon of

the PL peak shifts with changes in solvent polarity may be attributed to a reduced bandgap between the HOMO and LUMO resulting from solvation and the reorientation of polar molecules around the PL molecular group^{33,34}. The PL properties of CDs and DHQP was further investigated by tuning solvent polarity by mixing methanol and ethyl acetate. The maximum emission wavelength rapidly shifts toward the long wavelength with the addition of methanol (Fig. 5b). It depicts that a small amount (<2%) of methanol could cause a large redshift from 557 and 595 nm to 577 and 624 nm in DHQP solution, respectively, which is near 50% of the total spectral redshift in pure methanol. And this spectral shift rule is the same as the CDs solution. It is probably induced by hydrogen bonding of hydroxy group on alcohols solvent to the amino groups, rather than general solvent effect^{34,35}.

Moreover, the pH effect on the emissions of CDs and DHQP are presented in Fig. S6c, d. With the decrease of pH, the intensity of the PL emission peaks decreases. The emission at 598 nm has a more dramatic descent compared to the peak at 646 nm. When the pH is <4, the emission at 646 nm turns out to be the maximum (Fig. 5c). Overall, the emission of both CDs and DHQP keep the same tune as the pH. Both solvent and pH effects imply that the CDs and DHQP have a very similar optical response to the environment. Time-resolved PL spectra were employed to understand the exciton dynamics of CDs and DHQP. All samples were excited at 475 nm and the emission at 598 nm and 646 nm were probed (Figs. 5c and S7). DHQP molecule exhibits a single-exponential decay implying a single emissive state. The lifetime (τ) is 2.29 ns and 2.30 ns for emission at 598 and 646 nm, respectively. The decay traces of CDs are fitted with bi-exponential decays: the short lifetime (τ_1) is 2.24 ns ($A = 97.4\%$) and the long lifetime (τ_2) is 7.97 ns ($A = 2.6\%$), indicating that an extra process occurs in the red emissive CDs. The short lifetime is very close to the lifetime of DHQP. The long lifetime is attributed to the additional energy transfer from the green and blue units to the neighboring red ones³⁶. TEM images disclose that the CDs are composed of a few small conjugated units not a single particle (Fig. 2b). These results indicate both DHQP and CDs have the same origin.

On the other hand, the thermogravimetric analysis (TGA) was carried out to test the thermal stability of DHQP and CDs. As shown in Fig. S8, DHQP exhibits a sharp mass loss within 298 °C. However, the CDs show two significant mass loss peaks at 219 °C and 430 °C. The former may attribute to the removal of the functional group ($-\text{OH}$, $-\text{C}=\text{O}$, $-\text{NH}_2$) on the CDs surface, and the latter may be the further carbonization. Although DHQP and CDs have very similar optical properties, their thermal behavior is quite different, implying no free DHQP is contained in the CDs. To summarize the above results,

DHQP and CDs have similar PL properties, which is not originated from the free DHQP in CDs. Consequently, we deduce that DHQP is the fluorophore of this type CDs.

The formation process of CDs

Based on the above investigation, the three intermediates were produced in the reaction of oPD and CAT at 200 °C. They are 2,3-DAPN, phthalazine, and DHQP based on the HPLC-MS and ¹H NMR spectra. 2,3-DAPN is the dimer of oPD, and phthalazine is industrially synthesized from oPD and CAT.

To fully understand the formation process of DHQP, the oPD and CAT reacted with 2,3-DAPN and/or phthalazine at 100 °C, respectively. The PL spectra of reaction products are shown in Fig. S9, when CAT reacts with 2,3-DAPN and phthalazine, respectively, the PL emission wavelength is 550 and 536 nm, which is not the same as that of DHQP. In contrast, the product from oPD and 2,3-DAPN or phthalazine exhibits 600 and 650 nm emission peaks, which is similar to the DHQP. Accordingly, we speculate on the forming process of the CDs as shown in Fig. 6. First, oPD and CAT react to produce the intermediates (2,3-DAPN and phthalazine). Then, the intermediates further react with oPD to produce DHQP molecule. With the increase of temperature and the extension of reaction time, the molecule grows and carbonizes to form single-layer graphene embedded or connected DHQP molecules to CDs with an sp³ bond. The large version of CDs ¹H-NMR spectra (Fig. S10a) shows that the H of the benzene ring at the DHQP molecular edge significantly disappeared and became weaker. That indicates the benzene ring of the DHQP molecular edge could be incorporated into the structure of the conjugated CDs core (Fig. S10b). Finally, the single-layer graphene stack to zero-dimensional CDs.

Fluorescent mechanism of CDs

Despite the PL behavior of CDs and DHQP being pretty similar, the UV-vis spectra do not exhibit a high degree of similarity. Firstly, the solutions of CDs in ethanol show dark red and the DHQP solution shows purple (Fig. 7a), implying that they have different UV-vis absorption spectra. Notably, the CDs exhibit unique absorption bands at 318 and 366 nm (Fig. 7b), there are no absorption peaks in the DHQP. Considering the early reports^{30,37}, the peaks at 318 and 366 nm could be assigned to the $n-\pi^*$ transition of the $\text{C}=\text{N}$ and $\text{C}=\text{O}$ on the CDs surface. In addition, the absorption bands within 480–600 nm and 285 nm are the same as the DHQP, which could be assigned to the $n-\pi^*$ and $\pi-\pi^*$ transition of the molecular unit, respectively. The EEM spectra of DHQP and CDs are shown in Fig. 7c, d. The excitation wavelength of 285 nm gives more contribution to the emission at 600 nm for the DHQP. On the contrary, the absorption

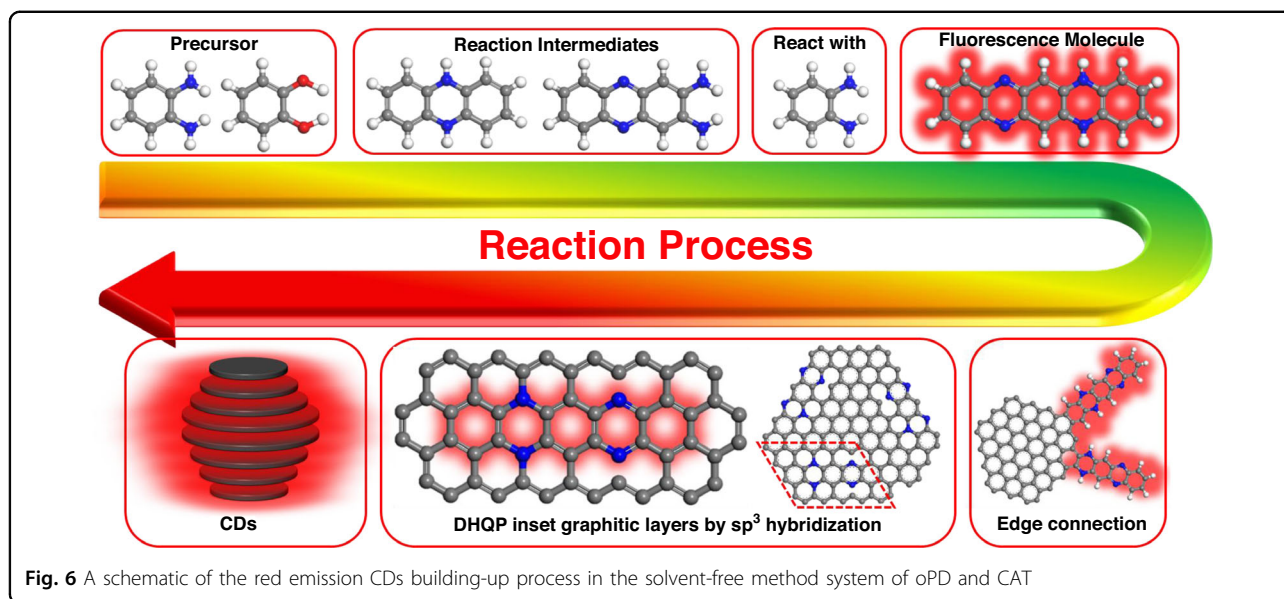


Fig. 6 A schematic of the red emission CDs building-up process in the solvent-free method system of oPD and CAT

band at 520 nm is the largest contributor to red emission. Figure 7e shows the fluorescent mechanism of DHQP, according to the Frank-Condon principle, the rate of electron transition is much higher than the nucleus motion, the nucleus will move to a new location to adapt to the geometrical configuration of electrons by vibration. Because the vibration is quantized, contributes to generating a lot of vibration energy levels ($V=1$, $V=2$, $V=3$, ...) in S_0 and S_1 states. Thus, the absorption at 500, 530, and 570 nm and emission bands at 600, 650, and 700 nm are the vibrational overtone bands, which correspond to absorption transition of 0-2, 0-1, 0-0, and emission transition of 0-0, 0-1, 0-2, respectively. The 0-1 transition is the most probable Frank-Condon transition^{30,38,39}. And the $\pi-\pi^*$ transition at 285 nm corresponds to the energy level transition between the S_0 and S_2 , the excited electron decay to the lowest vibration energy levels of S_1 through internal conversion (IC) and vibration relaxation, then return to S_0 through radiative emission transition of 0-0, 0-1, 0-2 (Fig. 7e). That is the reason why the excitation of 285 nm gives more contribution to the red emission.

In the case of CDs, DHQP was connected or embedded with carbon core by sp^3 matrix, and the fluorophore (DHQP) on the CDs is ultimately dominant in photoluminescent behaviors. The PL mechanism of 600, 650, and 700 nm emission excited by the 480–600 nm band is the same as those in DHQP. Intriguingly, the absorption peak at 285 nm has less contribution to the red emission, the probable reason is the excited electron may transfer to the energy level of CDs (S_n) which is mostly a non-radiation transition. The new excited energy levels (S_n) locate between S_1 and S_2 states related to the absorption band at 318 nm and 366 nm. The electron of

S_2 can transfer to the S_n of the CDs, which competes with internal conversion between S_2 and S_1 (Fig. 7f). This causes the PL intensity excited by the 285 nm band to be decreased.

Discussion

In summary, we synthesized the red emission CDs in high yield through the solvent-free method, and analyzed the origin of red emission and forming process of CDs. We separated the intermediates during the synthesis of the CDs by HPLC-MS. HPLC-MS and ¹H NMR spectra determine the intermediates containing the 2,3-DAPN, phthalazine, and DHQP. It reveals that the PL mechanism of this type of CDs should belong to molecule state fluorescent by comparing the PL properties of intermediates and the CDs. The PL emission and absorption are almost the same as the CDs in the visible region, the PL lifetime, PL change behavior in different solvents, and pH of DHQP are the same as the CDs, and the fluorophore of the CDs is DHQP, which incorporate into graphene or connect with graphene edge by sp^3 hybridization. During the PL emission of CDs, the electron of molecule state S_2 transfer to the S_n of CDs, resulting in the 285 nm exciting PL intensity at 480–600 nm band decreased. Our findings can potentially help understand the PL mechanism of the CDs that synthesized used oPD as a precursor and inspire a novel synthetic design to obtain red emission with tailored properties.

Materials and methods

Materials

o-Phenylenediamine, catechol, and aluminum chloride hexahydrate were purchased from Aladdin. phenazine and 2,3-diaminophenazine were purchased from Energy

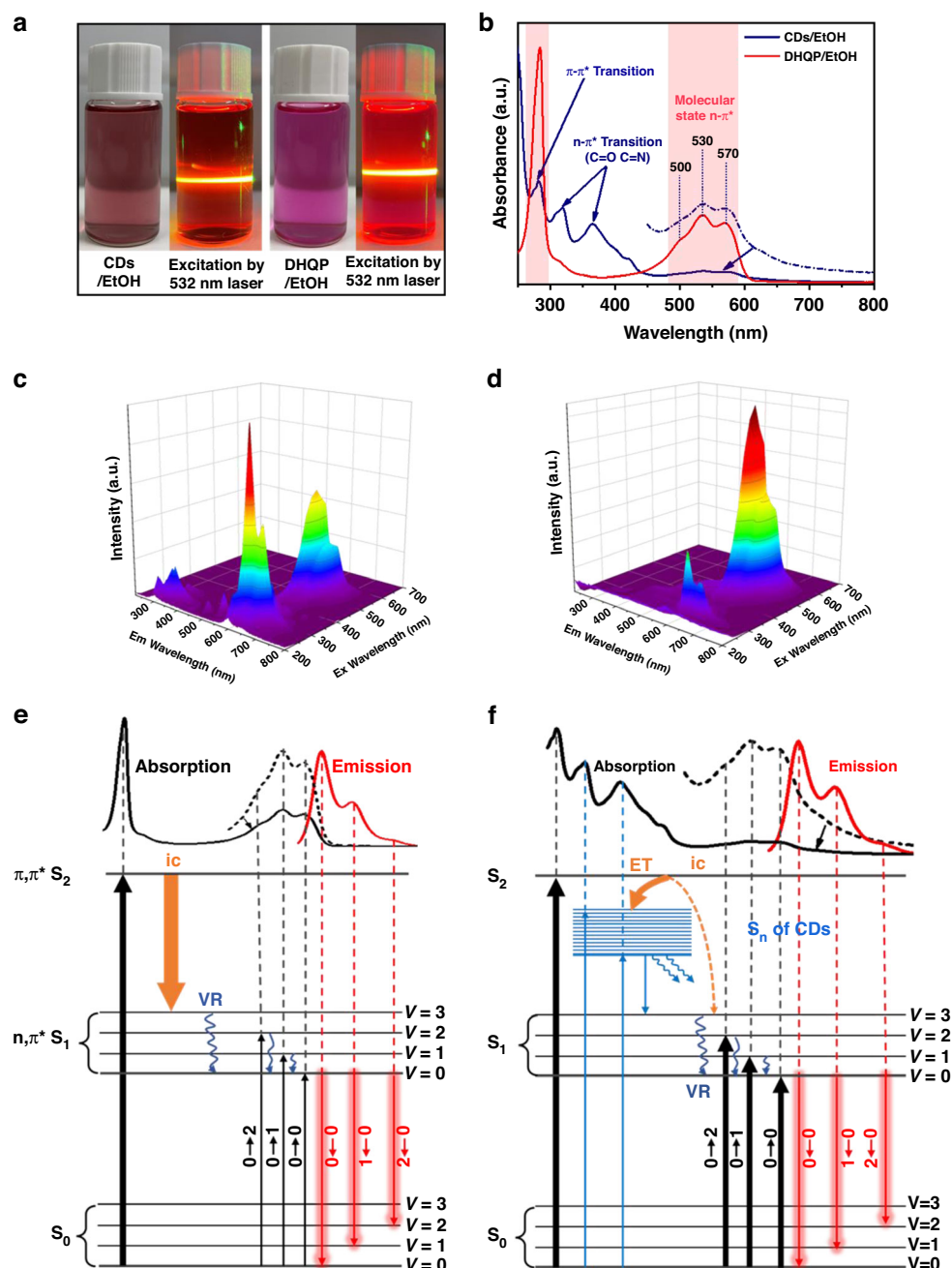


Fig. 7 The proposed fluorescent mechanism of DHQP and CDs. **a** Photo of the CDs and DHQP dissolved in EtOH, and the solutions were excited by a 532 nm laser. **b** The UV-vis contrast spectra of the DHQP and CDs. **c** and **d** EEM spectra of DHQP and CDs dissolved in ethanol. **e** and **f** Schematic diagram of the real experimental absorption and emission of DHQP and CDs. (ic: internal conversion, VR: vibration relaxation, ET: electron transfer)

Chemical and Heowns, respectively. All chemicals were used without further purification.

Synthesis of red emission CDs

The red emission CDs were prepared through the solvent-free method (Fig. 1a) the processes are as follows: 0.54 g (5 mmol) oPD, 0.55 g (5 mmol) CAT, and 0.08 g (0.33 mmol)

$\text{AlCl}_3 \cdot 6\text{H}_2\text{O}$ were mixed and ground uniformly in an agate mortar for 10 min. Then the mixture was transferred to a 30 mL Teflon-lined autoclave and heated for 12 h at 200 °C. Subsequently, the autoclave was taken out and cooled to room temperature naturally. The obtained carbonized powders were dissolved in an ethanol solution and filtered through a 0.22 μm polyethersulfone membrane to remove

large particles. And finally, the filtered solution was dialyzed in a dialysis bag with a cut-off of 3500 Da against DI water for 7 d, and the DI water was changed every 12 h.

Synthesis of samples 1, 2, and 3

Sample 1: 0.54 g oPD and 0.54 g CAT were mixed and ground uniformly in an agate mortar, and then the mixture was transferred to a 30 mL Teflon-lined autoclave for heating for 6 h at 100 °C. Sample 2: 0.54 g oPD and 0.54 g CAT were mixed and ground uniformly in an agate mortar, and then the mixture was transferred to a 30 mL Teflon-lined autoclave and heated for 12 h at 200 °C. Sample 3: Sample 2 was dissolved in 200 mL ethanol, the solution was centrifuged at 10,000 rpm for 10 mins, and the solid was selected to vacuum drying at 40 °C.

HPLC MS sample preparation

The Sample was dissolved in DMSO to form the 1 mg/mL solution. Then, the solution was diluted 100 times with water, acetonitrile and trifluoroacetic acid (95/5/0.1) to be measured. The model of HPLC-MS is Agilent 1290 Infinity/6460 LC/QQQ MS. C18 column (2.1 × 50 mm, 1.7 μm) was used to separate with the mobile phase A of 0.1% formic acid-water and mobile phase B of 0.1% formic acid-acetonitrile. The separation products were ionized in the electrospray ionization (ESI) and operated in positive mode.

Acknowledgements

This study was financially supported by the Beijing Municipal High-Level Innovative Team Building Program (grant no. IDHT20180504), the Beijing Outstanding Young Scientists Program (BJJWZYJH01201910005017), the National Natural Science Foundation of China (grant nos. 22272003, 21872001, 51801006, and 21805004), the Key Project of the National Natural Science Foundation of China (21936001 and 21801092), the Beijing Natural Science Foundation (grant no. 2192005), and the Beijing Municipal Science and Natural Science Fund Project (grant no. KM201910005016).

Author contributions

P.L. and Z.S. designed the experiment. P.L. prepared the samples and performed the measurement and characterization. All authors contributed to the discussion of the results. P.L. and Z.S. led the effort in the development of the manuscript. All authors have given approval to the final version of the manuscript.

Conflict of interest

The authors declare no competing interests.

Supplementary information The online version contains supplementary material available at <https://doi.org/10.1038/s41377-022-00984-5>.

Received: 9 April 2022 Revised: 31 August 2022 Accepted: 15 September 2022

Published online: 13 October 2022

References

- Xu, X. Y. et al. Electrophoretic analysis and purification of fluorescent single-walled carbon nanotube fragments. *J. Am. Chem. Soc.* **126**, 12736–12737 (2004).

- He, C. et al. The synthetic strategies, photoluminescence mechanisms and promising applications of carbon dots: Current state and future perspective. *Carbon* **186**, 91–127 (2022).
- Đorđević, L. et al. A multifunctional chemical toolbox to engineer carbon dots for biomedical and energy applications. *Nat. Nanotechnol.* **17**, 112–130 (2022).
- Miao, X. et al. Synthesis of carbon dots with multiple color emission by controlled graphitization and surface functionalization. *Adv. Mater.* **30**, 1704740 (2018).
- Qu, D. et al. Recent advance of carbon dots in bio-related applications. *J. Phys. Mater.* **3**, 022003 (2020).
- Zhang, M. et al. Fabrication of HA/PEI-functionalized carbon dots for tumor targeting, intracellular imaging and gene delivery. *RSC Adv.* **7**, 3369–3375 (2017).
- Wang, K. et al. Systematic safety evaluation on photoluminescent carbon dots. *Nanoscale Res. Lett.* **8**, 122 (2013).
- Ge, J. C. et al. Red emissive carbon dots for fluorescent, photoacoustic, and thermal theranostics in living mice. *Adv. Mater.* **27**, 4169–4177 (2015).
- Kasibabu, B. S. B. et al. One-step synthesis of fluorescent carbon dots for imaging bacterial and fungal cells. *Anal. Methods* **7**, 2373–2378 (2015).
- Li, J. P. et al. Imaging cellular aerobic glycolysis using carbon dots for early warning of tumorigenesis. *Adv. Mater.* **33**, 2005096 (2021).
- Zheng, M. et al. Integrating oxaliplatin with highly luminescent carbon dots: an unprecedented theranostic agent for personalized medicine. *Adv. Mater.* **26**, 3554–3560 (2014).
- Liu, J. J., Li, R. & Yang, B. Carbon dots: a new type of carbon-based nanomaterial with wide applications. *ACS Cent. Sci.* **6**, 2179–2195 (2020).
- Qu, D. et al. Tailoring color emissions from N-doped graphene quantum dots for bioimaging applications. *Light Sci. Appl.* **4**, e364 (2015).
- Ding, H. et al. Solvent-controlled synthesis of highly luminescent carbon dots with a wide color gamut and narrowed emission peak widths. *Small* **14**, e1800612 (2018).
- Li, H. T. et al. Water-soluble fluorescent carbon quantum dots and photocatalyst design. *Angew. Chem. Int. Ed.* **49**, 4430–4434 (2010).
- Sun, Y. P. et al. Quantum-sized carbon dots for bright and colorful photoluminescence. *J. Am. Chem. Soc.* **128**, 7756–7757 (2006).
- Kundele, E. V. et al. Amino functionalization of carbon dots leads to red emission enhancement. *J. Phys. Chem. Lett.* **10**, 5111–5116 (2019).
- Qu, D. et al. Highly luminescent S, N co-doped graphene quantum dots with broad visible absorption bands for visible light photocatalysts. *Nanoscale* **5**, 12272–12277 (2013).
- Miao, S. H. et al. Hetero-atom-doped carbon dots: Doping strategies, properties and applications. *Nano Today* **33**, 100879 (2020).
- Song, Y. B. et al. Investigation from chemical structure to photoluminescent mechanism: a type of carbon dots from the pyrolysis of citric acid and an amine. *J. Mater. Chem. C* **3**, 5976–5984 (2015).
- Kasprzyk, W. et al. Novel efficient fluorophores synthesized from citric acid. *RSC Adv.* **5**, 34795–34799 (2015).
- Qu, D. & Sun, Z. C. The formation mechanism and fluorophores of carbon dots synthesized via a bottom-up route. *Mater. Chem. Front.* **4**, 400–420 (2020).
- Liu, Y. X., Jia, Q. & Zhou, J. Recent advance in near-infrared (NIR) imaging probes for cancer theranostics. *Adv. Ther.* **1**, 1800055 (2018).
- Wu, Y. S. et al. White-light-emitting melamine-formaldehyde microspheres through polymer-mediated aggregation and encapsulation of graphene quantum dots. *Adv. Sci.* **6**, 1801432 (2019).
- Zhu, Z. J. et al. Red carbon dots: optical property regulations and applications. *Mater. Today* **30**, 52–79 (2019).
- Wang, Y. Y., Su, Q. & Yang, X. M. Exploration of the synthesis of three types of multicolor carbon dot originating from isomers. *Chem. Commun.* **54**, 11312–11315 (2018).
- Jiang, K. et al. Red, green, and blue luminescence by carbon dots: Full-color emission tuning and multicolor cellular imaging. *Angew. Chem.* **54**, 5360–5363 (2015).
- Ding, H. et al. Large scale synthesis of full-color emissive carbon dots from a single carbon source by a solvent-free method. *Nano Res.* **15**, 3548–3555 (2022).
- Zhang, Q. et al. Photoluminescence mechanism of carbon dots: triggering high-color-purity red fluorescence emission through edge amino protonation. *Nat. Commun.* **12**, 6856 (2021).
- Soni, N. et al. Absorption and emission of light in red emissive carbon nanodots. *Chem. Sci.* **12**, 3615–3626 (2021).

31. Verma, N. C., Yadav, A. & Nandi, C. K. Paving the path to the future of carbogenic nanodots. *Nat. Commun.* **10**, 2391 (2019).
32. Yang, J. et al. Proton nuclear magnetic resonance spectroscopy of active hydrogen. *Univ. Chem.* **34**, 82–88 (2019).
33. Sato, R, Iso, Y. & Isobe, T. Fluorescence solvatochromism of carbon dot dispersions prepared from phenylenediamine and optimization of red emission. *Langmuir* **35**, 15257–15266 (2019).
34. Lakowicz, J. R. *Principles of Fluorescence Spectroscopy* (Springer, 2006).
35. Takashi, T. The photoassociation of 1- and 2-acetylanthracenes with methanol. *Bull. Chem. Soc. Jpn* **55**, 1761–1767 (1982).
36. Zhao, Y. Y. et al. Tailoring the photoluminescence excitation dependence of the carbon dots via an alkali treatment. *J. Phys. Chem. Lett.* **10**, 4596–4602 (2019).
37. Shamsipur, M. et al. Resolving the multiple emission centers in carbon dots: from fluorophore molecular states to aromatic domain states and carbon-core states. *J. Phys. Chem. Lett.* **9**, 4189–4198 (2018).
38. Niu, M. S. et al. Molecular packing correlated fluorescence in TIPS-pentacene films. *Electronics* **49**, 340–346 (2017).
39. Kao, K. C. *Dielectric Phenomena in Solids*. (Academic Press, New York, 2004).